Submitted to *Journal of Alloys and Compounds*

Research Article

Microstructures and mechanical properties of nano-C and in-situ Al_2O_3 reinforced aluminum matrix composites processed by equal-channel angular pressing

Jinmei Chen[a,b], Xiaosong Jiang[a,b], Lan Lyu[a,b], Yanjun Li[c*], Pål Christian[c], Hongliang Sun[a,b], Rui Shu[d]*

[a]Key Laboratory of Advanced Technologies of Materials, Ministry of Education, Chengdu 610031, China

[b]School of Materials Science and Engineering, Southwest Jiaotong University, Chengdu Sichuan 610031, China

[c]Department of Materials Science and Engineering, Norwegian University of Science and Technology, Trondheim 7491, Norway

[d]Forschungszentrum Jülich GmbH Institut für Energie-und Klimaforschung Plasmaphysik (IEK-4)52425 Jülich, Germany

*Corresponding author: xsjiang@swjtu.edu.cn (X.S. Jiang), Tel./Fax: +86-28-87600779 OR yanjun.li@ntnu.no (Y.J. Li), Tel./Fax: +47 73551206.

Abstract

In this paper, the powder metallurgy method was used to prepare nano-C and in-situ Al_2O_3 hybrid reinforced Al matrix composites, the grain size was refined and the dispersion of reinforcements was improved by equal-channel angular pressing (ECAP). There were twin Si and slip steps in the composites reinforced by 0.75% CNTs, 0.25% GNPs and Al_2O_3 by 3 ECAP passes. The interface between CNTs and the matrix was closely bonded. The γ-Al_2O_3 particles and fibers were generated by the in-situ method, and the nucleation and interfacial orientation of Al_2O_3 were discussed. With the increase of ECAP passes, the electrical and mechanical properties of the composites were

improved. The resistivity of 0.5% GNPs reinforced the composites by 3 ECAP passes was the lowest, which was 3.64×10^{-8} Ωm. The maximum hardness of 1.0% CNTs reinforced the composites after 3 ECAP passes was 321.9 HV. The compressive strength the composites were improved compared with that of Al-Si alloy. The strengthening mechanism of ECAP treated Al matrix composites was summarized as dislocation strengthening, dispersion strengthening, grain boundary strengthening and load transfer.

Keywords: nano-C; Al matrix composites; equal-channel angular pressing; interfacial orientation; strengthening mechanism

1. Introduction

Lightweight Al matrix composites with low density, excellent mechanical and electrical properties have been widely used in automobile manufacturing and aerospace fields, such as automotive brakes, jet engine gears and cutting tools [1]. The reinforcements of metal matrix composites mainly include particle phase and fiber phase. The particle reinforced phases include Al_2O_3 [2, 3], SiC [4-7], TiB_2 [8, 9]. Ceramic particle reinforced metal matrix composites have the advantages of high strength and good plastic toughness of metal materials as well as high hardness and good wear resistance of ceramic particles. The main fiber phases are carbon nanotubes (CNTs) [10-12] and graphene nanoplatelets (GNPs) [13, 14], CNTs have Young's modulus of 1.8 TPa, bending strength of 14.2 GPa, and excellent electrical properties [10-12]. Its unique properties are related to the highly symmetrical structure. GNPs have excellent mechanical properties, electrical conductivity and thermal conductivity [13], it can improve the electrical and mechanical properties of metal materials [15].

Nano-C and Al_2O_3 reinforced Al matrix composites have attracted much attention, the strengthening mechanism can be summarized as follows: grain boundary strengthening, dispersion strengthening, load transfer and dislocation strengthening [16]. Phuong et al. [17] found that the hardness of the CNTs reinforced Al matrix composites is higher than that of pure Al, and the grain size of the composites is significantly smaller. Chen et al. [11] believed that CNTs can play a role in dispersion strengthening when the length of CNT was far less than the dislocation. The

strengthening effect of GNP is mainly load transfer. Guo et al. [18] pointed out that the amorphous transition region between CNTs and Al matrix is conducive to load transfer. The effect of dislocation strengthening is related to the shape of the reinforcements, and the effect of the plate is greater than that of the fiber than that of the spherical particle [19]. Chen [20] prepared the Al-CNTs-γ-Al_2O_3 composites with excellent tensile properties, and calculated the contribution of γ-Al_2O_3, CNTs and ultrafine-grained Al matrix to tensile strength.

Although Al matrix composites with nano-C and Al_2O_3 have excellent properties, the preparation of the materials is still facing challenges. For instance, the nano-C is easy to agglomerate [10, 13], the wettability between the agglomerated nano-C and Al matrix is poor, and the interface is easy to produce holes and microcracks. The large strain produced by the large plastic deformation technology can disperse nano-C, improve the density and refine the grain size [17]. Currently, major plastic deformation technologies applied to metal matrix composites mainly include high-pressure torsion [21-23], ECAP [1, 24, 25], cyclic extrusion compression [26, 27], accumulative roll bonding [28, 29]. ECAP has the characteristics of uniform deformation, high density, clean process, simple process and low cost, so it has great potential to prepare the metal matrix composites [30]. Besides, the Al_2O_3 ceramic phase can strengthen the Al matrix, but it has poor wettability with the metal matrix, and the in-situ reaction can effectively improve the interface structure [2].

In this paper, nano-C and in-situ Al_2O_3 hybrid reinforced Al matrix composites were prepared by ball milling and hot isostatic pressing (HIP) sintering. ECAP technology was used to improve the density of the composites, refine the grain size and optimize properties. The interfacial bonding structure between reinforcements and Al matrix was analyzed, the electrical and mechanical properties were measured, and the strengthening mechanisms were discussed in detail based on the experimental results.

2 Experimental procedure

2.1 Preparation of Al matrix composites

Based on the preparation method of Shu et al. in our team, the as-prepared Al matrix composites were prepared [31]. The main raw materials of the composites are

Al powder, SiO_2 powder, CNTs, GNPs. The diameter of spherical pure Al powder is about 16-30 μm and the purity is 99.7%. SiO_2 is mainly used to provide O for in-situ Al_2O_3 and form Al-Si alloy matrix containing 5% Si, and the mass ratio of Al: SiO_2 is 9.47:1. The particle size of SiO_2 powder is 13 μm and the purity is 99.9%. CNTs and GNPs are used as reinforcements. The length of CNTs is 10-30 μm, the diameter is 20-30 nm, and the purity is 95%. The GNPs lamellae are less than 10 layers, and the purity is 99.8%. Rutin solution and gallic acid solution graft hydrophilic groups on the surface of nano-C to achieve surface modification [31, 32]. Al powder, SiO_2 powder, dispersed CNTs and GNPs were matched according to the composition of the Al-5% Si alloy enhanced by 1.0% CNTs, 0.5% GNPs and 0.75% CNTs+0.25% GNPs. A planetary ball milling (WL-1) was used to mix the powder at a speed of 350 rpm for 1 h. The mixed slurry was placed in a vacuum freeze dryer (FD-A-50) at - 50 ℃ for 24 h. Cold isostatic press (KJY C) was used to preform the composites powders. The composites were sintered by HIP (QIH-15) at 800℃ with a pressure of 70 MPa, for 0.5 h [31].

In order to refine grain and improve the mechanical and electrical properties of the composites, ECAP technology was used to process the composites. The ECAP machine (MTS-311) has two 10 mm × 10 mm cross-section channels (vertical channel and horizontal channel). The as-prepared composites were lubricated with MoS_2. At room temperature, the extrusion speed of ECAP was 0.5mm /s, exerting a force of 200 KN and passing through path A. The extrusion passes were 0, 1, 2 and 3, respectively. The preparation process of the composites is shown in Fig. 1.

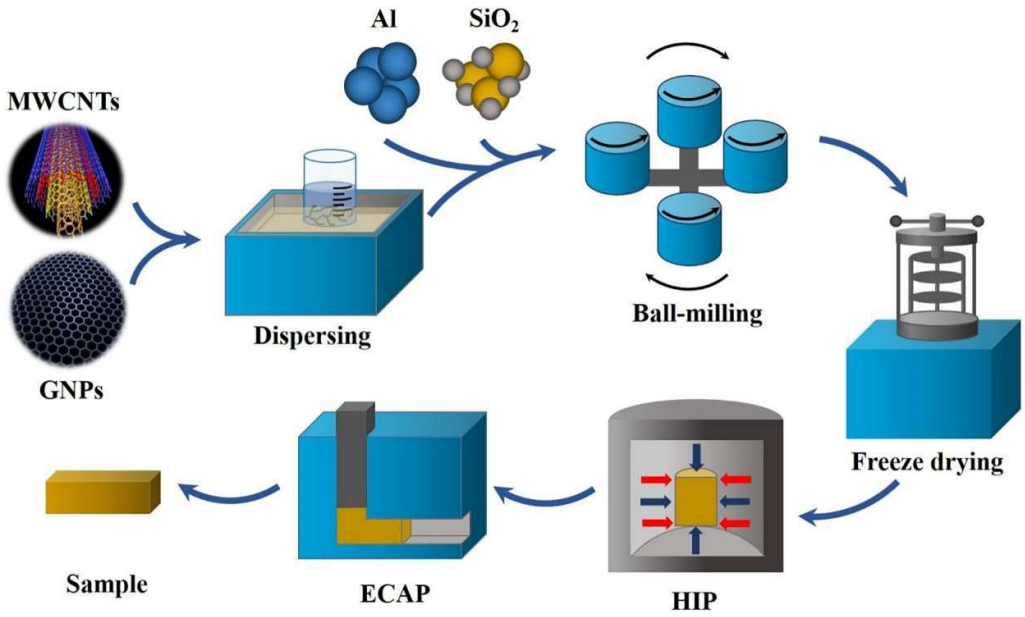

Fig. 1. The schematic diagram of the preparation of the Al matrix composites

2.2 Microstructural characterization and mechanical testing

The X-ray diffraction (XRD, X.Pert Pro-MPD) was used to analyze the microstructure of the composites. The distribution of the enhancements were observed by optical microscope (OM, Zeis Axio Imager. Aim). The surface microstructure of the composites was further observed by scanning electron microscope (SEM, JEOL JSM-7001F), and EDS analyzed the point composition, and judged the phase composition. Transmission electron microscope (TEM, JM-2100F) was used to observe the morphology and distribution of reinforcements, and analyze the interface structure between reinforcements and the matrix. The density of the composite was measured by the Archimedes principle. The hardness of the composite was tested by a microhardness tester (HXD-1000TM) with load of 100 gf for 10s, and the sampling method was shown in Fig. 2. The universal testing machine (WDW-3100) was used to test the compressive properties of the Al-Si alloy and the composites. The electrical property of the composites was measured by a conductivity tester (Sigmatest 2.06).

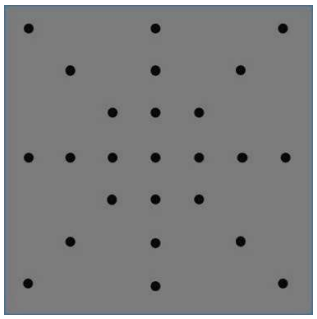

Fig. 2. The sampling method for testing hardness of the composites

3 Results and Discussion

3.1 Microstructure analysis

Fig. 3 shows the XRD spectra of Al matrix composites enhanced by 1.0% CNTs with 0 ECAP pass and 3 ECAP passes. The composites consist of four phases, Al, Si, γ-Al_2O_3 and Al_4C_3, and the peak strength of Al_2O_3 and Al_4C_3 is very small. Al_2O_3 is generated by the in-situ reaction between Al and SiO_2, and the reaction equation is shown in formula (1). Compared with XRD standard card, γ- Al_2O_3 was obtained by in-situ reaction. Woo et al. [33] also successfully prepared Al_2O_3 reinforced the Al matrix composites by in-situ reaction of Al and SiO_2. The process of ball milling leads to the transformation of CNTs from the complete C wall to C atom [18, 34], the free C and Al are easy to react to form Al_4C_3. However, the amount of free C provided by ball milling is limited, so the content of Al_4C_3 is very small.

$$4Al + 3SiO_2 \rightarrow 2Al_2O_3 + 3Si \quad (1)$$

Besides, no new phase is detected after ECAP, indicating that there is no phase transformation, but the peak strength changes significantly. The strength of $\{111\}_{Al}$ and $\{311\}_{Al}$ increases, while the peak strength of $\{200\}_{Al}$ decreases obviously, which shows that the grains of $\{200\}_{Al}$ are broken and refined by ECAP, and the shear strain leads to the grain turning and moving. Therefore, more and more grains are distributed along with the $\{111\}_{Al}$ and $\{311\}_{Al}$ planes.

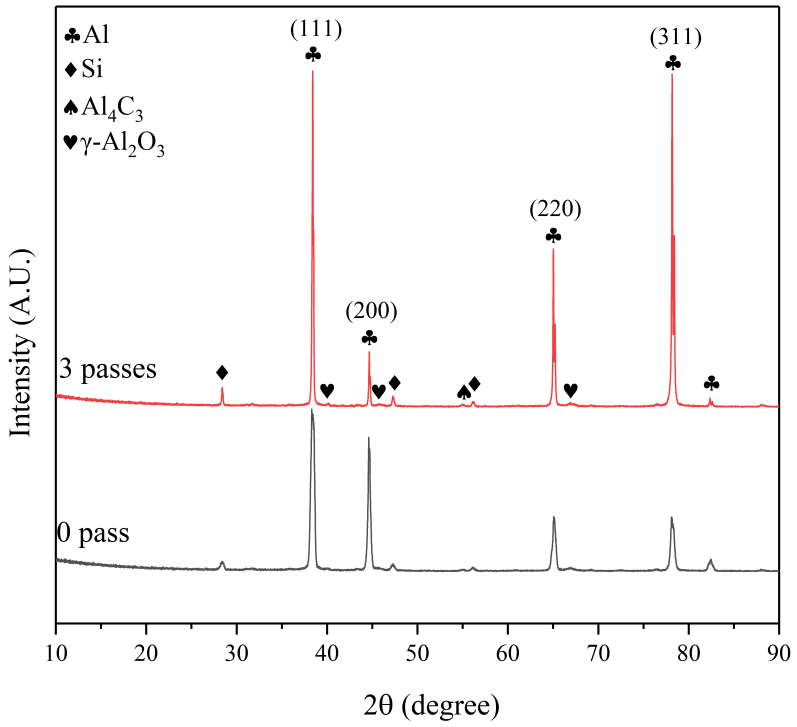

Fig. 3. XRD spectra of the composites reinforced by 1.0% CNTs and Al_2O_3

Fig. 4 shows the microstructure of the composites reinforced by nano-C and Al_2O_3. The OM images of 0 ECAP pass and 3 ECAP passes of the composites reinforced by 0.5% GNPs and Al_2O_3 are shown in Fig. 4a and b, GNPs aggregates are observed in the as-prepared composites which are easy to fall off during polishing. In the composite of 3 ECAP passes, the size of black GNPs aggregates decreases significantly, and GNPs are uniformly distributed in the matrix. ECAP produced a large shear strain, broken the GNPs aggregates and improved the dispersion of GNPs.

Fig. 4c-f are the SEM images of the composites reinforced by 1.0% CNTs and Al_2O_3 with 0, 1, 2 and 3 ECAP passes, respectively. In Fig. 4c, the white granular phase, dark gray phase and black phase are distributed in the matrix. According to the EDS results, the uniformly distributed white particles are Al_2O_3, the grain size is about 3 μm, and in-situ Al_2O_3 particles present a fan shape (the circle area) and multilateral shape, dispersive Al_2O_3 particles can play an effective role in dispersion strengthening [3]. Al_2O_3 and the black phase are also observed in Fig. 4d. In Fig. 4e, the EDS results show that the black phase is nano-C and the dark gray phase is Si generated by in-situ reaction

which is distributed at the interface of Al. The EDS result in Fig. 4f further proves that the white particle phase is Al_2O_3, and the size of Al_2O_3 particles is consistent with that in Fig. 4c of 0 ECAP pass, indicating Al_2O_3 are not destroyed by ECAP. Arab et al. [35] suggested that ECAP improved the interface structure of ceramic phase and matrix, which is conducive to the load transfer and generated more dislocations to improve the effect of dislocation strengthening.

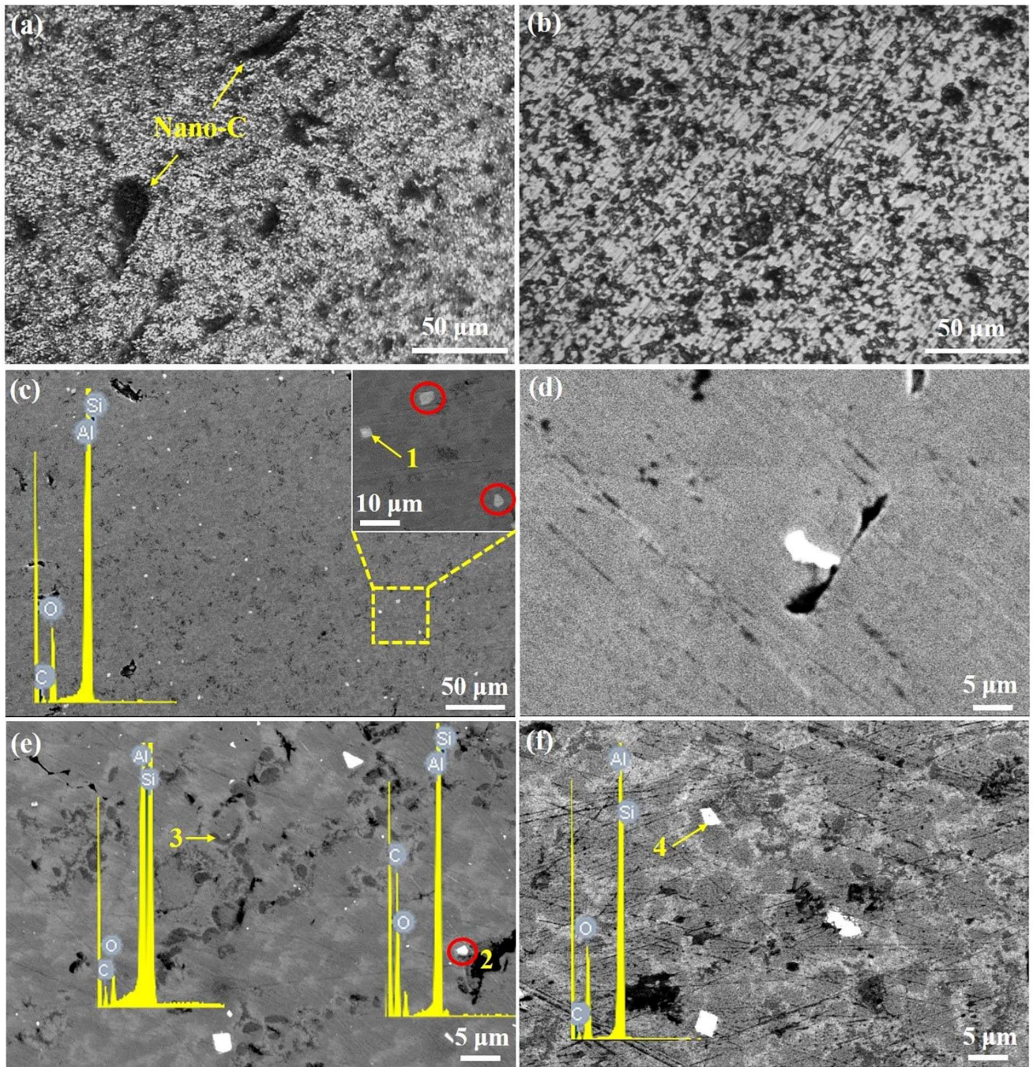

Fig. 4. Microstructure morphology of the composites, (a, b) OM images of the Al matrix composites reinforced by 0.5% GNPs and Al_2O_3 of ECAP 0 pass and 3 passes, (c-f) SEM images of Al matrix composites reinforced by 1.0% CNTs and Al_2O_3 of 0, 1, 2 and 3 ECAP passes

Fig. 5 shows the TEM results of Al matrix composites reinforced by 0.75% CNTs,

0.25% GNPs and Al_2O_3 by 3 ECAP passes. In Fig. 5a, the EDS result shows that the content of Si is 87%, indicating that the black strips material is Si with an obvious twin structure. There are flake GNPs in the grain boundary of Al-Si matrix. Fig. 5b is the SAED result of point 1, which can separate two sets of symmetrical diffraction patterns, further proving that the black stripe material is Si with a twin structure. Some Si atoms diffuse into the Al grains and nucleated into strip Si, while others nucleate and grow before diffusion to form granular Si, which adhered to the surface of Al grains [36].

In Fig. 5c and d, a large number of slip steps are observed in the matrix. Because a large number of dislocations are generated during the ECAP process and slip to the particle surface. According to TEM results, the plastic deformation mechanism of the composites are deduced. Al with a FCC structure has many slip systems. Therefore, in the early stage of ECAP plastic deformation, dislocation slip is the main deformation mechanism. Because of the barrier effect of the interface and reinforcements on the dislocation, dislocation stacking is caused. As the plastic deformation continues to increase, twin Si is induced, and the deformation mechanism is mainly twinning. The twin Si provides a supplementary deformation mechanism, which is beneficial to improve the mechanical properties of the composites.

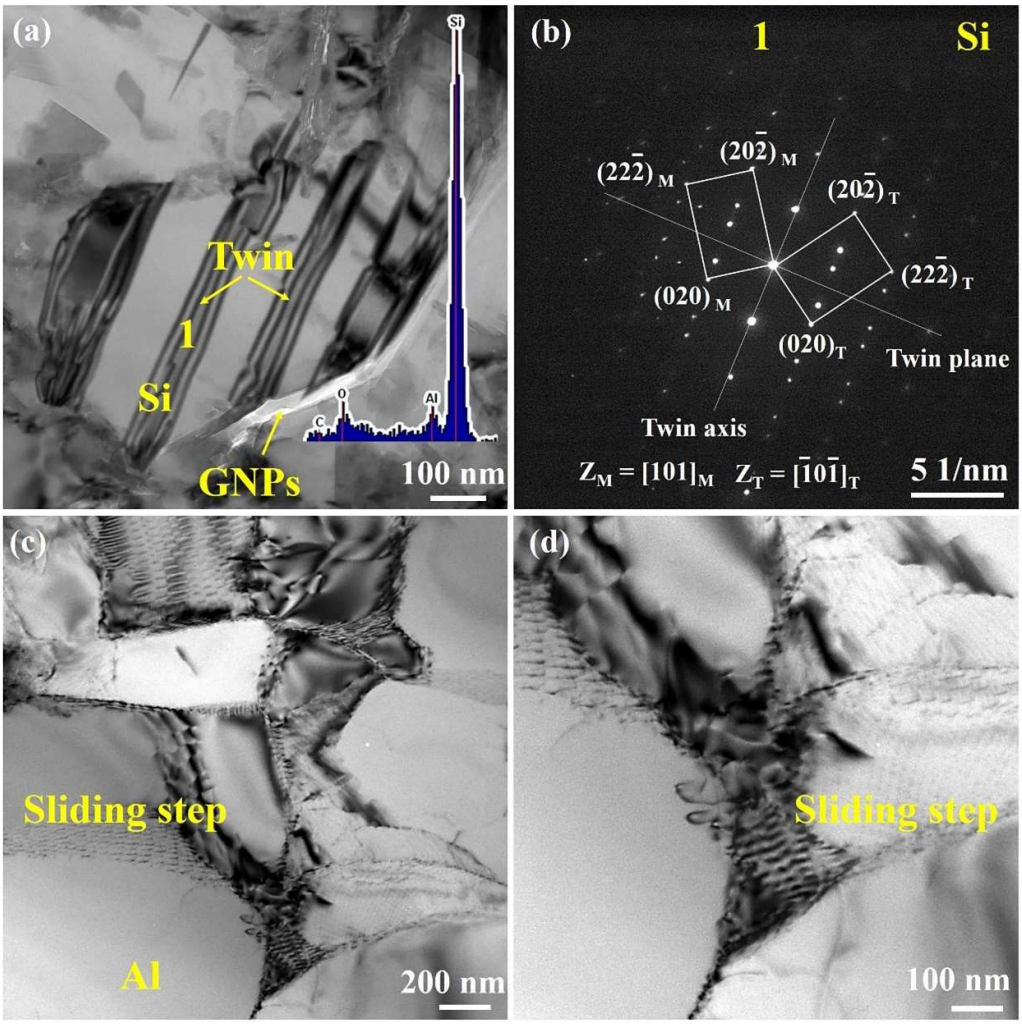

Fig. 5. TEM of the Al matrix composites enhanced by 0.75% CNTs, 0.25% GNPs and Al_2O_3 by 3 ECAP passes

Fig. 6 shows the TEM images of Al_2O_3 in the Al matrix composites reinforced by 0.75% CNTs, 0.25% GNPs and Al_2O_3 by 3 ECAP passes. In Fig. 6a, fibers and granular materials are observed around the gray-white Al matrix. The boxed positions in Fig. 6a are enlarged in Fig. 6b and c. The EDS result in Fig. 6b suggests that the fibers are Al_2O_3, which are randomly distributed and interlacing without an obvious orientation relationship. The EDS result in Fig. 6c indicates that the particle phase also is Al_2O_3. Al_2O_3 particles are distributed along with the interface of Al matrix and have a pinning effect on grain boundary, which prevent grain boundary movement of Al in the high-temperature sintering process, prevent grain growth and refine grain. The α-Al_2O_3 requires a high temperature of 1200℃ to produce, while the formation temperature of

γ-Al_2O_3 is relatively low. The nucleated Al_2O_3 particles grow into Al_2O_3 fibers with sufficient parent phase [37], and the sintering temperature in this paper is 800℃, so both particle and fiber phase are γ-Al_2O_3, and this conclusion is consistent with the XRD results.

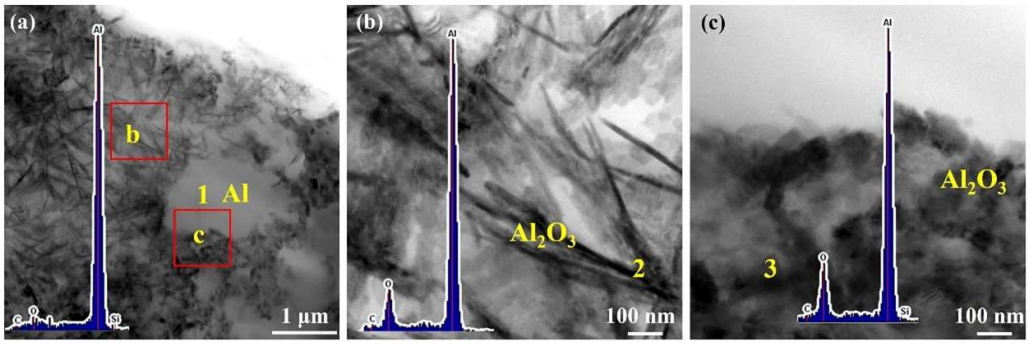

Fig. 6. TEM and EDS results of the Al matrix composites reinforced by 0.75% CNTs, 0.25% GNPs and Al_2O_3 by 3 ECAP passes

Fig. 7 shows the interface structure between Al_2O_3 and matrix. In Fig. 7a, the agglomerated nano-C is entangled with Al_2O_3 particles. In Fig. 7b, EDS proves that the particle phase is Al_2O_3, and it's similar to the fan shape, which is consistent with SEM results. The interface is clear and narrow, which also proves the advantage of the in-situ method to prepare enhancements. Besides, a single CNT with discrete distribution and a single GNP with wrinkled surface were observed, which suggests the dispersion of nano-C can be improved by chemical modification.

Fig. 7c shows that the diameter of Al_2O_3 short fiber is about 20 nm, and the ECAP process does not make the short fiber bend or break, so the short fiber Al_2O_3 has high strength. Fig. 7d is a HRTEM image of the box region in Fig. 7c. Al_2O_3 fiber is closely bound to the matrix with a clean interface. Besides, the interface is not smooth and presents a serrate shape, which can increase the friction force, prevent the fiber pulled out and improve the strength of the composites. The crystal spacing of Al_2O_3 fiber is 0.20 nm. Qu [37] prepared Al matrix composites reinforced by in-situ γ-Al_2O_3 whisker, the average diameter of the whisker is 20 nm, the crystal spacing is 0.20 nm, and this paper is consistent with it.

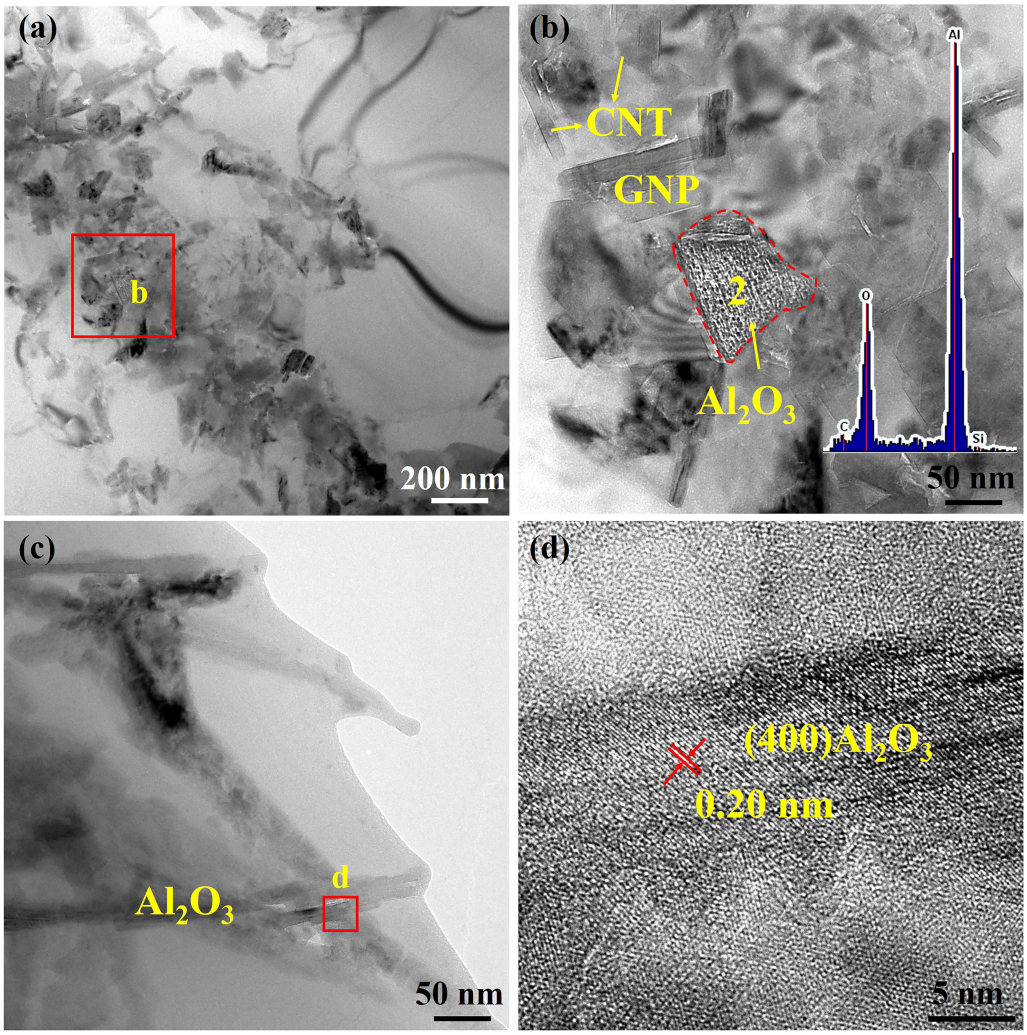

Fig. 7. TEM images of the Al composites reinforced by 0.75% CNTs, 0.25% GNPs and Al_2O_3 by 3 ECAP passes, (a, b) Al_2O_3 particles, (c, d) Al_2O_3 fiber.

Fig. 8 is the TEM images of the composites enhanced by 0.75% CNTs, 0.25% GNPs and Al_2O_3 by 3 ECAP passes. The EDS result in Fig. 8a shows that the gray-white material is agglomerated nano-C. CNTs are distributed at the grain boundary with obvious root structure and bent during preparation. Nano-C is closely bonded with the matrix without obvious pores. Fig. 8b is the SAED pattern at point 1, and the diffraction pattern is concentric rings, which indicates that C is polycrystalline because of the entanglement of CNTs and GNPs. Fig. 8c indicates that flake GNPs distribute at the edge of CNTs aggregates. In Fig. 8d, CNTs are embedded in Al matrix.

Fig. 8e and f are the HRTEM of the interface between nano-C and matrix. In Fig. 8e, a single curved CNT is observed. The interface between CNT and matrix is tightly

bonded, clean and without brittle phase. The layer spacing of CNTs is 0.37 nm, which is little larger than other reports [38-40]. ECAP produces large strains that cause bending of CNTs, slightly increasing the layer spacing of CNTs. In Fig. 8f, the bond between CNTs and Al matrix is close and there seem to be an amorphous transition layer at the interface [15, 18].

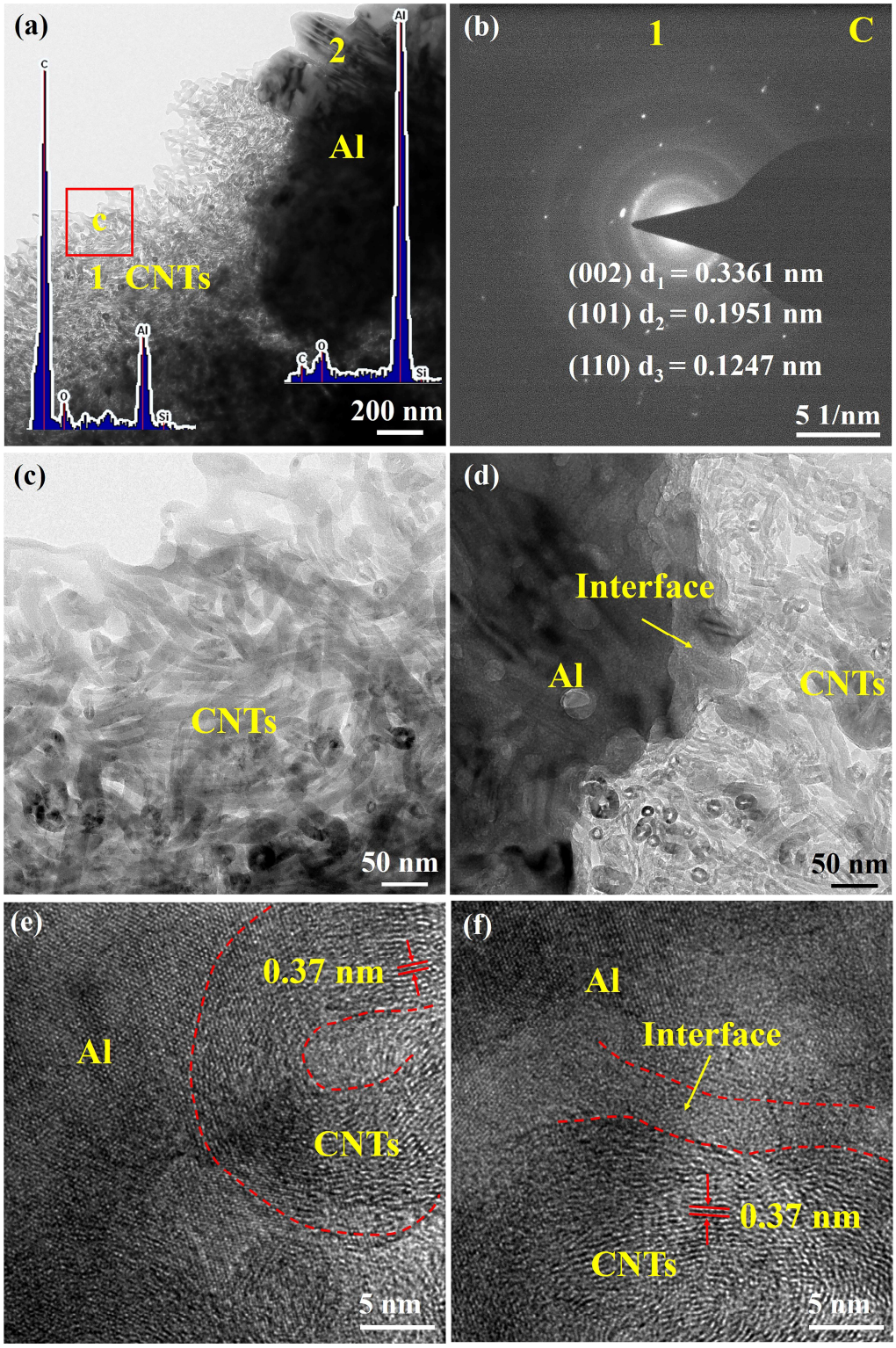

Fig. 8. TEM images of the interface between CNTs and Al matrix

3.2 The nucleation and interface of Al_2O_3

In the process of preparation, Al and SiO_2 reacted to form Si and Al_2O_3. Under the

experimental conditions, the new phase nucleates and grows by heterogeneous nucleation. During the sintering process, Al and SiO_2 diffuse each other, and the parent phase provides the wall of heterogeneous nucleation for the new phase, and the new phase is attached to the parent phase nucleation and grows at the expense of the parent phase. No SiO_2 is observed by XRD or SEM, indicating that the in-situ reaction is thorough and SiO_2 is almost completely consumed.

Si and Al_2O_3 particles are distributed along the grain boundary of Al in the SEM and TEM images. The free enthalpy of the system at the interface is high, especially at the high-angle grain boundary (HAGB), the atom mismatch degree is high, the structure is loose, and the bond is seriously distorted or even broken, and the energy stored can reduce the heterogeneous nucleation work, which is more conducive to the nucleation and make the system thermodynamic stable [41]. Al_2O_3 particles are observed to be fan-shaped and polygonal in the microscopic images in Fig. 4 and Fig. 7, which is related to the orientation of the interface. Fig. 9 is a schematic diagram of the interface relationship between Al_2O_3 and Al grains. The energy at the grain boundary, dislocation and other defects are high, so Al_2O_3 is easy to nucleate at the defect of Al grain [42, 43].

In Fig. 9a, Al_2O_3 particles nucleate along the HAGB. The grains Al 1 and Al 2 on both sides of the HAGB are non-coherent. The lattice constant of γ-Al_2O_3 is 8, that of Al is 4, and that of γ-Al_2O_3 is just twice of Al. When Al_2O_3 adheres to Al for nucleation, one side of the Al_2O_3 may have a certain orientation relationship with Al 1 [44, 45], forming a flat interface similar to coherent or semi-coherent, which can reduce the interface energy and the nucleation work. On the other side of Al_2O_3 particles, due to the influence of HAGB, the mismatch degree of Al 1 and Al 2 is large. The interface between Al_2O_3 and Al 2 must be a non-coherent interface with a poor matching degree. During the nucleation and growth process, the interface is an arc to reduce the interface area.

Besides, some of the Al_2O_3 particles in this paper are polygonal, mostly quadrilateral, as shown in Fig. 9b. A series of dislocations form the low-angle grain boundary (LAGB), so part of the Al_2O_3 nucleate along the LAGB and most of the atoms on both sides of LAGB match well. Therefore, interfaces of nucleated Al_2O_3 and Al

grains on both sides are flat which is similar to coherent or semi-coherent, so Al_2O_3 is a quadrilateral. At the reaction temperature, the Al_2O_3 particles nucleate. When the parent phase is sufficient, the Al_2O_3 fibers nucleate and grow on the basis of the Al_2O_3 particles in the heat preservation process [37]. Adequate SiO_2 supports the Al_2O_3 fibers with large aspect ratio to grow on the basis of particles. When the parent phase is insufficient, SiO_2 is consumed before growing into Al_2O_3 fibers, only Al_2O_3 particles can be obtained, and the fanlike and quadrilateral states of nucleated Al_2O_3 are retained.

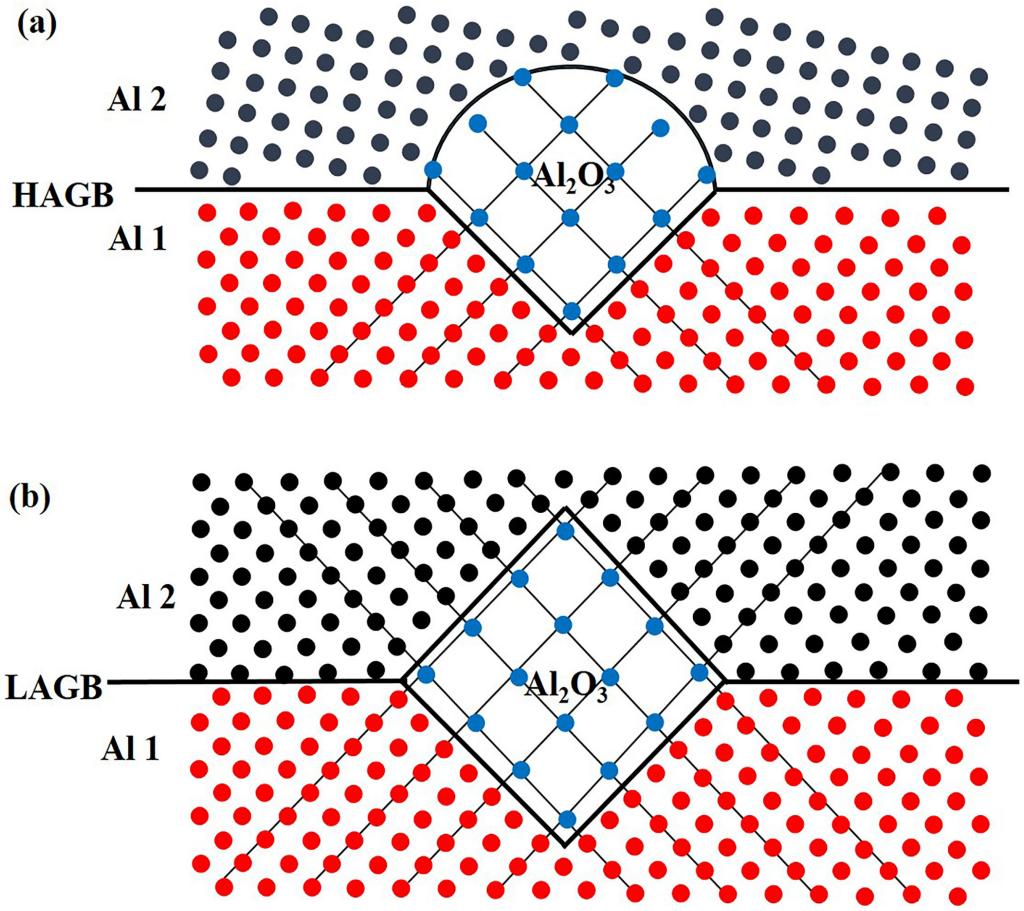

Fig. 9. The relationship between nucleation and interface orientation of Al_2O_3

3.3 Performance test analysis

Fig. 10 shows the relative density of the composites. In the as-prepared composites, the relative density of 1.0% CNTs reinforced the composite is the lowest, because the thermal expansion coefficient of nano-C is greatly different from that of Al [46], the relative density decrease with the increase of nano-C. In addition, CNTs are easier to agglomerate than GNPs due to their large aspect ratio, and agglomeration reduces the

density [47]. Compared with the as-prepared composites, the relative density of the composites increases with the increase of ECAP passes. ECAP produces shear strain, breaks up the aggregates, disperses the reinforcement and fill the void in the matrix to improve the relative density [24, 48]. After 3 ECAP passes, the relative density of all composites are above 99.8%, and the composite with 0.75% CNTs and 0.25% GNPs is still the highest, which is 99.96%.

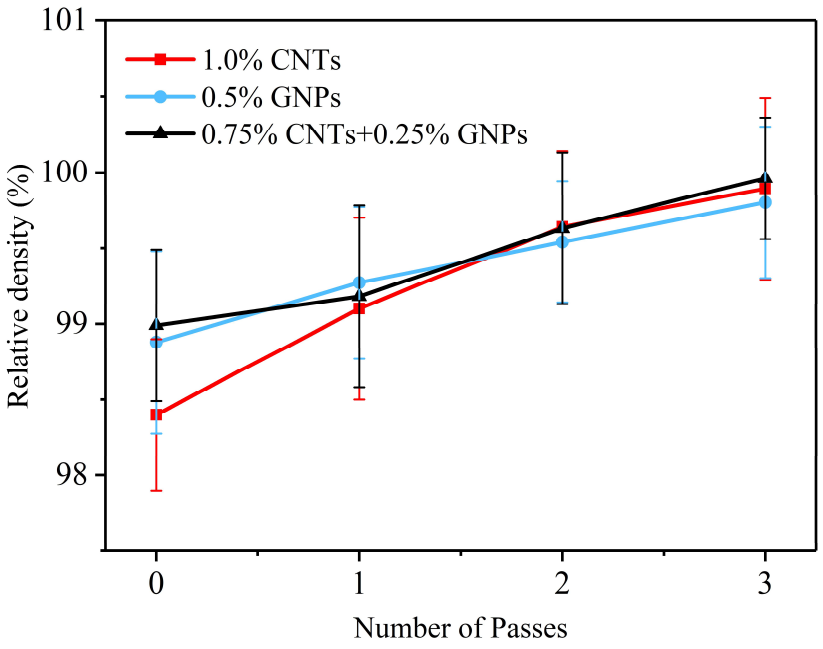

Fig. 10. The curve of the relative density of the Al matrix composites reinforced by nano-C and Al_2O_3 by ECAP

Fig. 11 is a diagram of resistivity of the composites with different ECAP passes. The resistivity of the composite reinforced by 0.5% GNPs is the lowest, and that of composites with1.0% CNTs is the highest. The higher the content of nano-C is, the higher the porosity of the composites is. The holes cause electron scattering, hinder the directional movement of electrons and increase the resistivity. Besides, the aspect ratio of CNT is larger, and CNT has excellent electrical property only in the axial direction [49], while GNP is a two-dimensional material with extremely high electrical conductivity [38]. After ECAP treatment, the resistivity of the composites decreased, and the resistivity of 0.5% GNPs reinforced the composites by 3 ECAP passes is 3.64

$\times 10^{-8}$ Ωm. ECAP breaks nano-C aggregates, reduce the porosity, make the directional movement of electrons more smoothly, and thus improve the electrical conductivity.

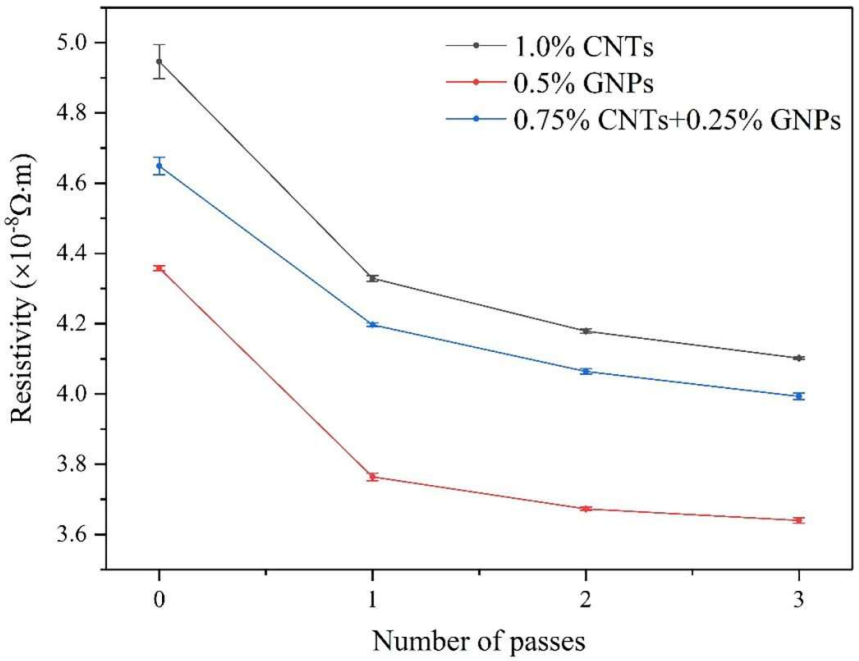

Fig. 11. The curve of the resistivity of the Al matrix composites by ECAP

Fig. 12 is a diagram of the microhardness distribution of 1.0% CNTs reinforced the composites by ECAP. The hardness distribution diagram of the as-prepared composites is uniform in color, and the average hardness value is 76.6 HV. The maximum hardness of 1.0% CNTs reinforced Al prepared by Van Trinh is about 58 HV [50], which is much lower than that of the as-prepared 1.0% CNTs reinforced Al-Si alloy in this paper, because Si is conducive to improving the hardness of Al. As the number of passes of ECAP increases, the hardness of the sample increases. After 3 ECAP passes, the minimum hardness of the sample reaches 109.3 HV and the hardness at (3, 0) reaches 321.9 HV. The hardness at the center does not increase as much as that at the edge, and the center hardness of the composite is small and the edge hardness is large. This phenomenon becomes more obvious with the increase of the passes of ECAP.

The hardness distribution is related to the porosity and strain gradient [51, 52]. The higher the porosity, the lower the hardness; the greater the strain, the higher the hardness.

With the increase of extrusion passes, the strain accumulates and produces a strong shear effect, which reduces the porosity of the sample edge and increases the density, so the hardness of the edge is large. Also, when the shear stress reaches the yield strength, the sample breaks and recrystallizes, refine the grain and improve the hardness. At the same time, the nano-C dispersed more evenly, the enhancement effect is better. However, the shear strain at the center is small and the strengthening effect is small, which results in the difference of hardness between the center and the edge. Zare et al. [1] prepared the Al matrix composites by ECAP and also found that the edge hardness of the sample was large, and pointed that the hardness heterogeneity is related to the flow rate of the material during the ECAP process.

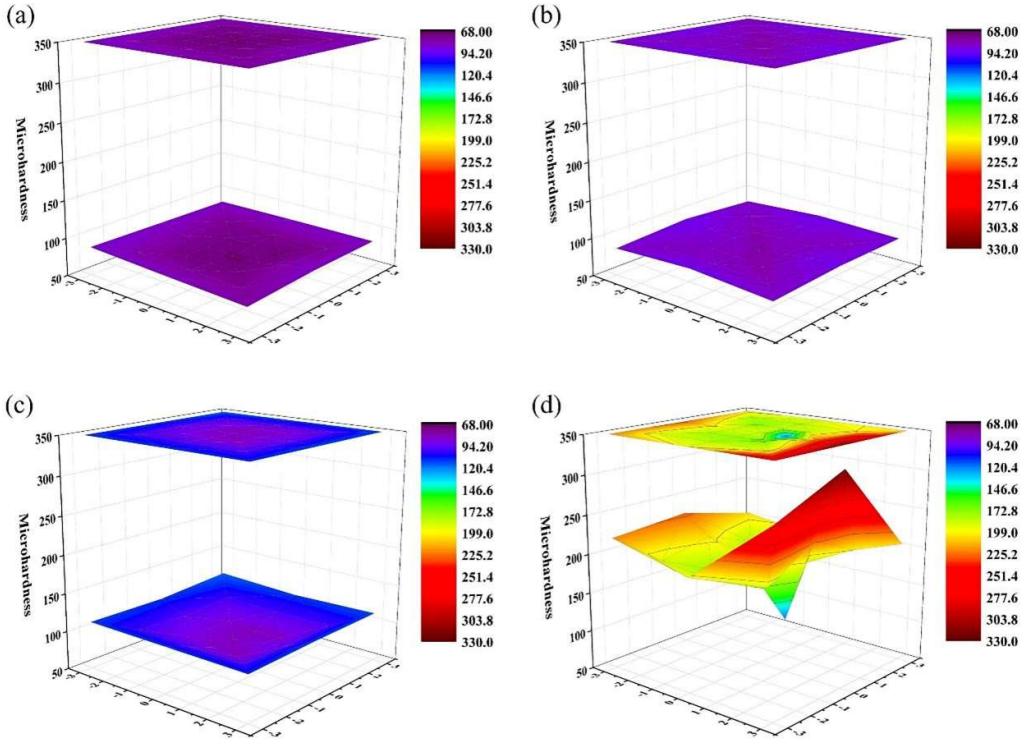

Fig. 12. The microhardness distribution of the Al matrix composites reinforced by 1.0% CNTs with 0, 1, 2 and 3 ECAP passes, respectively (the hardness on the top is a two-dimensional representation, and the hardness on the bottom is a three-dimensional representation)

Fig. 13 is the compressive stress-strain curve of Al-Si alloy and the Al matrix composites after 3 ECAP passes. The compressive strength of Al-Si alloy is 330MPa

and the compression ratio is 31%. After 3 ECAP passes, the compressive strength of the composites with 1.0% CNTs, 0.5% GNPs, 0.75% CNTs+0.25% GNPs are 397MPa, 395MPa and 392MPa respectively, and the compression ratio is 33%, 40% and 35%, respectively, indicating that the compressive strength and compression ratio of the composites are improved compared with that of Al-Si alloy. On the one hand, the addition of CNTs and GNPs can play the role of load transfer and improve the strength effectively [18, 39, 40]. On the other hand, compared with the compressive strength of Al matrix composites without ECAP treatment prepared by Shu of our research group [31], the compressive strength in this paper is all improved. The ECAP increases the dislocation density, and the dislocation movement is blocked at the interface and the reinforcement, resulting in the formation of substructure and grain refinement. The dynamic recovery in the ECAP process improves the strength and toughness of the composites [1, 25].

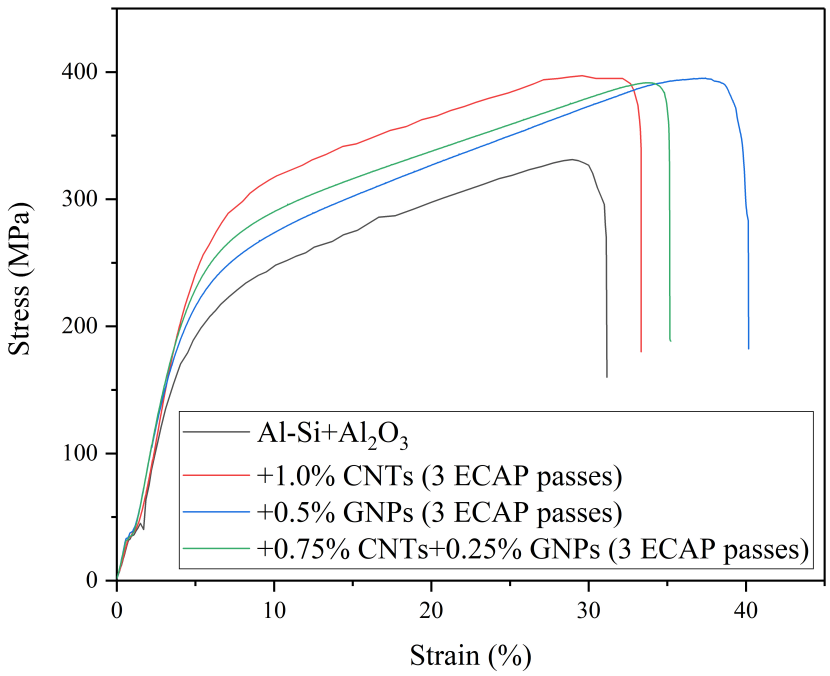

Fig. 13. The compressive stress-strain curve of Al-Si alloy and the Al matrix composites after 3 ECAP passes

3.4 Strengthening mechanism analysis

In this paper, the reinforcements of the Al matrix composites include CNTs, GNPs, Al_2O_3 fiber and particles. According to the experimental results, the strengthening mechanism of the composites by ECAP mainly includes load transfer, dislocation strengthening, dispersion strengthening and grain boundary strengthening. The schematic diagram of the strengthening mechanism is shown in Fig. 14. The load transfer plays a very important strengthening role for CNTs and GNPs, as shown in Fig. 14a. A large number of studies have indicated that the amorphous transition region between the nano-C and Al matrix can strengthen the interfacial structure, and the load can be transferred more effectively from the matrix to the fiber reinforcements [15, 18, 23, 38]. Strengthening value of load transfer ($\Delta\sigma_{LT}$) can be calculated by the formula (2-4) [16, 39].

$$\Delta\sigma_{LT} = \sigma_m V_m + \sigma_f V_f (1 - L_c/(2L)) - \sigma_m \qquad L > L_c \tag{2}$$

$$\Delta\sigma_{LT} = \sigma_m V_m + \sigma_f V_f (L_c/(2L)) - \sigma_m \qquad L \leq L_c \tag{3}$$

$$L_c = \sigma_f d_f/(2\tau_m) \tag{4}$$

σ_m and σ_f represent the strength of matrix and reinforcements, V_m and V_f are the volume fraction of matrix and reinforcements. L denotes the actual length of the fiber, and L_c denotes the critical length. d_f is the average diameter of the reinforcements τ_m is the shear modulus of the matrix.

In TEM results, a large number of dislocations were observed. The dislocations mainly come from two parts, one is the difference of thermal expansion coefficient between reinforcements and matrix, which leads to the increase of initial dislocation density [1]. The thermal expansion coefficient of Al is $24 \times 10^{-6} \cdot C^{-1}$, that of Al_2O_3 is $7.92 \times 10^{-6} \cdot C^{-1}$, and that of nano-C is $2 \times 10^{-6} \cdot C^{-1}$. During sintering and cooling, the different expansion and contraction degree between reinforcements and Al matrix leads to strain mismatch at the interface, which increases the initial dislocation density and promotes dislocation strengthening. The other part is that ECAP produces large plastic deformation and increases dislocation density, as shown in Fig. 14b. As ECAP goes on, the dislocations begin to move. When the moving dislocations encounter the fine Al_2O_3 particles, the dislocations bypass the nanoparticles and leave a dislocation ring around the nanoparticles to achieve the effect of dispersion strengthening, as shown

in Fig. 14c. The dispersion strengthening value ($\Delta\sigma_{DS}$) can be calculated by the formula (5) [21].

$$\Delta\sigma_{DS} = MGb \ln(\pi d_t/4b/(2\pi\gamma\sqrt{1-v})) \quad (5)$$

M is the Taylor factor, G is the shear modulus of the matrix, b is the burgers Vector, d_t is the average diameter of the reinforcement, v is Poisson's ratio, and γ is the particle spacing of the reinforcement.

In the early stages of ECAP, when the moving dislocations meet large Al_2O_3 particles, CNTs, GNPs and interfaces, the dislocations are blocked and piled up. The accumulated dislocations evolve into dislocation walls and micro shear bands, resulting in grain orientation differences and the formation of subgrain boundaries (misorientation < 2°). With the development of ECAP, the degree of dislocation accumulation increases, and the subgrains rotate, resulting in the further increase of misorientation. The subgrain boundaries transform into LAGBs (2° < misorientation < 15°), and then into HAGBs (misorientation > 15°) [53, 54], and the grain is refined, as shown in Fig. 14d. In addition, the large shear stress produced by large plastic deformation can break the grains, ECAP further achieve the effect of grain boundary strengthening. Contribution of grain boundary strengthening to hardness (ΔH_{GR}) can be calculated by the Hall-Petch equation, in formula (6).

$$\Delta H_{GR} = K (d_c^{-0.5} - d_m^{-0.5}) \quad (6)$$

K is the Hall-Petch constant of the matrix, d_c and d_m represent the average grain size of the composite and matrix.

The nucleation, growth and grain refinement of HAGBs are closely related to the dynamic recovery process, which is mainly controlled by the climbing of edge dislocation and the cross slip of screw dislocation. The climbing of the edge dislocation is a diffusion process, and the effect is significant at high temperature. However, the ECAP process in this paper is at room temperature, so the dynamic recovery process in this paper is mainly related to the cross-slip of the screw dislocation. Generally speaking, the larger the stacking fault energy is, the more likely the screw dislocation is to occur cross-slip. Al has a high stacking fault, so the cross-slip mechanism

dominates the dynamic recovery process [55]. Dislocation proliferation and dynamic recovery compete with each other to control the mechanical properties of the composites.

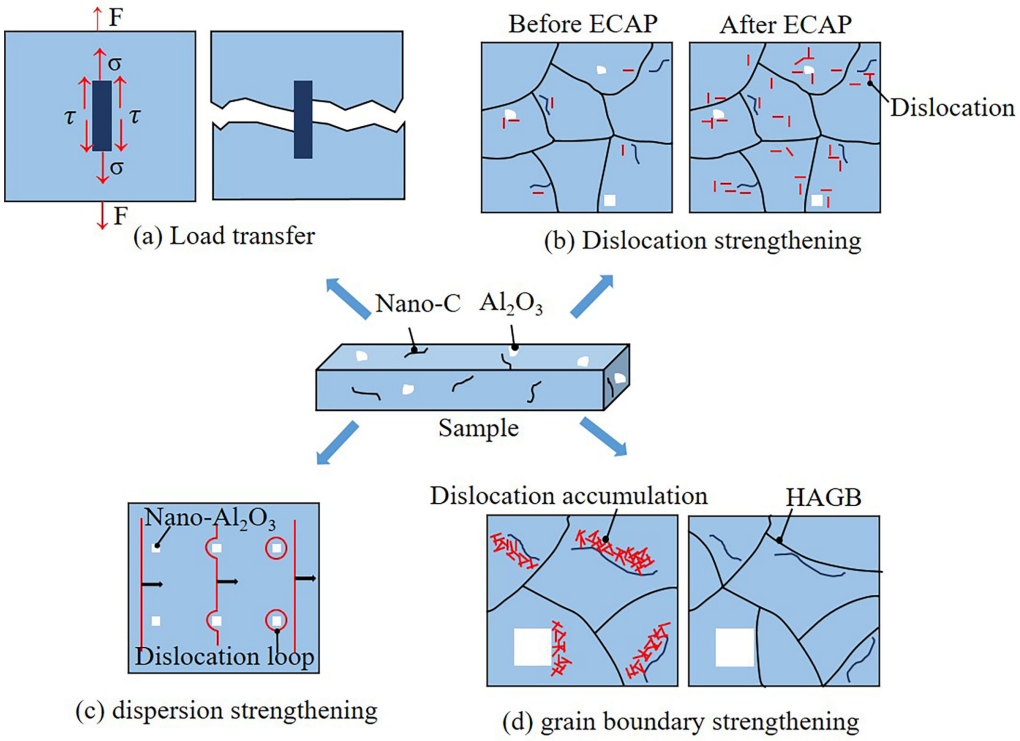

Fig. 14. The strengthening mechanism of the Al matrix composites

4 Conclusion

In this paper, nano-C and in-situ Al_2O_3 hybrid reinforced Al matrix composites were prepared by ball milling and HIP sintering, the properties of the composites were improved by ECAP, the structure of the composites was analyzed, and the electrical and mechanical properties of the composites were tested.

Strip twin Si and a large number of slip steps were observed in the composites reinforced by 0.75% CNTs, 0.25% GNPs and Al_2O_3 by 3 ECAP passes. The interface between CNTs and the matrix was closely bonded. The shear strain generated by ECAP broke the GNPs aggregates and improved the nano-C dispersion. The γ-Al_2O_3 particles and fiber were formed by in-situ reaction, and the morphology of Al_2O_3 particles was fan-shaped and quadrilateral, which is related to the characteristics of particle nucleation and the orientation of interface.

With the increase of ECAP passes, the density, electrical conductivity and hardness of the composites increase. After 3 ECAP passes, the density of composites reached over 99.8%. The resistivity of 0.5% GNPs reinforced the composites by 3 ECAP passes was 3.64×10^{-8} Ωm. The hardness of the as-prepared composites with CNTs was 76.6HV. After 3 ECAP passes, the maximum hardness reached 321.9 HV. The compressive strength and compression ratio of the composites after 3 ECAP passes are improved compared with that of Al-Si alloy. The strengthening mechanism of the composites is summarized as dislocation strengthening, dispersion strengthening, grain boundary strengthening and load transfer.

Acknowledgments

This work was supported by Key Laboratory of Infrared Imaging Materials and Detectors, Shanghai Institute of Technical Physics, Chinese Academy of Sciences ((No. IIMDKFJJ-19-08), R&D Projects Funding from the Research Council of Norway (No.263875/H30), China Postdoctoral Science Foundation (No. 2015M570794, No. 2018T110993).

References

[1] H. Zare, M. Jahedi, M.R. Toroghinejad, M. Meratian, M. Knezevic, Microstructure and mechanical properties of carbon nanotubes reinforced aluminum matrix composites synthesized via equal-channel angular pressing, Materials Science and Engineering: A 670 (2016) 205-216. https://doi.org/10.1016/j.msea.2016.06.027

[2] H. Wang, G. Li, Y. Zhao, G. Chen, In situ fabrication and microstructure of Al_2O_3 particles reinforced aluminum matrix composites, Materials Science and Engineering: A 527(12) (2010) 2881-2885. https://doi.org/10.1016/j.msea.2010.01.022

[3] Y.C. Kang, S.L.I. Chan, Tensile properties of nanometric Al_2O_3 particulate-reinforced aluminum matrix composites, Materials Chemistry and Physics 85(2-3) (2004) 438-443. https://doi.org/10.1016/j.matchemphys.2004.02.002

[4] M.P. Reddy, R.A. Shakoor, G. Parande, V. Manakari, F. Ubaid, A.M.A. Mohamed, M. Gupta, Enhanced performance of nano-sized SiC reinforced Al metal matrix nanocomposites synthesized through microwave sintering and hot extrusion techniques, Progress in Natural Science: Materials International 27(5) (2017) 606-614. https://doi.org/10.1016/j.pnsc.2017.08.015

[5] L.Y. Chen, J.Q. Xu, H. Choi, M. Pozuelo, X.L. Ma, S. Bhowmick, J.M. Yang, S. Mathaudhu, X.C. Li, Processing and properties of magnesium containing a dense uniform dispersion of nanoparticles, Nature 528(7583) (2015) 539-543. https://doi.org/10.1038/nature16445

[6] Q. Zhang, G.Q. Chen, G.H. Wu, Z.Y. Xiu, B.F. Luan, Property characteristics of a AlNp/Al composite fabricated by squeeze casting technology, Materials Letters 57(8)

(2003) 1453-1458. https://doi.org/10.1016/S0167-577x(02)01006-6

[7] S. Duan, D. Zhu, J. Dong, X. Lu, D. Ding, W. Zhou, F. Luo, Enhanced mechanical and microwave absorption properties of SiCf/SiC composite using aluminum powder as active filler, Journal of Alloys and Compounds 790 (2019) 58-69. https://doi.org/10.1016/j.jallcom.2019.03.171

[8] R.S. Jiang, W.H. Wang, G.D. Song, Z.Q. Wang, Experimental investigation on machinability of in situ formed TiB_2 particles reinforced Al MMCs, Journal of Manufacturing Processes 23 (2016) 249-257. https://doi.org/10.1016/j.jmapro.2016.05.004

[9] P. Senthil, T. Selvaraj, Sivaprasad, Influence of turning parameters on the machinability of homogenized Al–Cu/TiB_2 in situ metal matrix composites, The International Journal of Advanced Manufacturing Technology 67(5-8) (2013) 1589-1596. https://doi.org/10.1007/s00170-012-4592-3

[10] W. Zhou, T. Yamaguchi, K. Kikuchi, N. Nomura, A. Kawasaki, Effectively enhanced load transfer by interfacial reactions in multi-walled carbon nanotube reinforced Al matrix composites, Acta Materialia 125 (2017) 369-376. https://doi.org/10.1016/j.actamat.2016.12.022

[11] B. Chen, J. Shen, X. Ye, L. Jia, S. Li, J. Umeda, M. Takahashi, K. Kondoh, Length effect of carbon nanotubes on the strengthening mechanisms in metal matrix composites, Acta Materialia 140 (2017) 317-325. https://doi.org/10.1016/j.actamat.2017.08.048

[12] C. He, N. Zhao, C. Shi, X. Du, J. Li, H. Li, Q. Cui, An Approach to Obtaining Homogeneously Dispersed Carbon Nanotubes in Al Powders for Preparing Reinforced Al-Matrix Composites, Advanced Materials 19(8) (2007) 1128-1132. https://doi.org/10.1002/adma.200601381

[13] H. Porwal, P. Tatarko, S. Grasso, C. Hu, A.R. Boccaccini, I. Dlouhy, M.J. Reece, Toughened and machinable glass matrix composites reinforced with graphene and graphene-oxide nano platelets, Science and Technology of Advanced Materials 14(5) (2013) 055007. https://doi.org/10.1088/1468-6996/14/5/055007

[14] A. Nieto, A. Bisht, D. Lahiri, C. Zhang, A. Agarwal, Graphene reinforced metal

and ceramic matrix composites: a review, International Materials Reviews 62(5) (2016) 241-302. https://doi.org/10.1080/09506608.2016.1219481

[15] Z. Li, Q. Guo, Z. Li, G. Fan, D.B. Xiong, Y. Su, J. Zhang, D. Zhang, Enhanced Mechanical Properties of Graphene (Reduced Graphene Oxide)/Aluminum Composites with a Bioinspired Nanolaminated Structure, Nano Letters 15(12) (2015) 8077-83. https://doi.org/10.1021/acs.nanolett.5b03492

[16] X. Zhang, S. Li, B. Pan, D. Pan, S. Zhou, S. Yang, L. Jia, K. Kondoh, A novel strengthening effect of in-situ nano Al_2O_3w on CNTs reinforced aluminum matrix nanocomposites and the matched strengthening mechanisms, Journal of Alloys and Compounds 764 (2018) 279-288. https://doi.org/10.1016/j.jallcom.2018.06.006

[17] D.D. Phuong, P.V. Trinh, N.V. An, N.V. Luan, P.N. Minh, R.K. Khisamov, K.S. Nazarov, L.R. Zubairov, R.R. Mulyukov, A.A. Nazarov, Effects of carbon nanotube content and annealing temperature on the hardness of CNT reinforced aluminum nanocomposites processed by the high pressure torsion technique, Journal of Alloys and Compounds 613 (2014) 68-73. https://doi.org/10.1016/j.jallcom.2014.05.219

[18] B. Guo, M. Song, J. Yi, S. Ni, T. Shen, Y. Du, Improving the mechanical properties of carbon nanotubes reinforced pure aluminum matrix composites by achieving non-equilibrium interface, Materials & Design 120 (2017) 56-65. https://doi.org/10.1016/j.matdes.2017.01.096

[19] Z. Zhang, H.M. Urbassek, Dislocation-based strengthening mechanisms in metal-matrix nanocomposites: a molecular dynamics study of the influence of reinforcement shape in the Al-Si system, Computational Materials Science 145 (2018) 109-115. https://doi.org/10.1016/j.commatsci.2017.12.063

[20] B. Chen, K. Kondoh, J.S. Li, M. Qian, Extraordinary reinforcing effect of carbon nanotubes in aluminium matrix composites assisted by in-situ alumina nanoparticles, Composites Part B: Engineering 183 (2020). https://doi.org/10.1016/j.compositesb.2019.107691

[21] H. Asgharzadeh, S.H. Joo, H.S. Kim, Consolidation of Carbon Nanotube Reinforced Aluminum Matrix Composites by High-Pressure Torsion, Metallurgical and Materials Transactions A 45(9) (2014) 4129-4137. https://doi.org/10.1007/s11661-014-

2354-6

[22] T. Tokunaga, K. Kaneko, Z. Horita, Production of aluminum-matrix carbon nanotube composite using high pressure torsion, Materials Science and Engineering: A 490(1-2) (2008) 300-304. https://doi.org/10.1016/j.msea.2008.02.022

[23] L. Zhao, H. Lu, Z. Gao, Microstructure and Mechanical Properties of Al/Graphene Composite Produced by High-Pressure Torsion, Advanced Engineering Materials 17(7) (2015) 976-981. https://doi.org/10.1002/adem.201400375

[24] R. Casati, A. Fabrizi, A. Tuissi, K. Xia, M. Vedani, ECAP consolidation of Al matrix composites reinforced with in-situ γ-Al_2O_3 nanoparticles, Materials Science and Engineering: A 648 (2015) 113-122. https://doi.org/10.1016/j.msea.2015.09.025

[25] H. Zare, M. Jahedi, M.R. Toroghinejad, M. Meratian, M. Knezevic, Compressive, shear, and fracture behavior of CNT reinforced Al matrix composites manufactured by severe plastic deformation, Materials & Design 106 (2016) 112-119. https://doi.org/10.1016/j.matdes.2016.05.109

[26] L. Zhang, Q. Wang, W. Liao, W. Guo, B. Ye, W. Li, H. Jiang, W. Ding, Effects of cyclic extrusion and compression on the microstructure and mechanical properties of AZ91D magnesium composites reinforced by SiC nanoparticles, Materials Characterization 126 (2017) 17-27. https://doi.org/10.1016/j.matchar.2017.01.008

[27] W. Guo, Q. Wang, B. Ye, X. Li, X. Liu, H. Zhou, Microstructural refinement and homogenization of Mg–SiC nanocomposites by cyclic extrusion compression, Materials Science Engineering: A 556 (2012) 267-270. https://doi.org/10.1016/j.msea.2012.06.086

[28] M. Reihanian, E. Bagherpour, M.H. Paydar, On the achievement of uniform particle distribution in metal matrix composites fabricated by accumulative roll bonding, Materials Letters 91 (2013) 59-62. https://doi.org/10.1016/j.matlet.2012.09.043

[29] R. Jamaati, M.R. Toroghinejad, Manufacturing of high-strength aluminum/alumina composite by accumulative roll bonding, Materials Science and Engineering: A 527(16-17) (2010) 4146-4151. https://doi.org/10.1016/j.msea.2010.03.070

[30] M.H. Azar, B. Sadri, A. Nemati, S. Angizi, M.H. Shaeri, P. Minarik, J. Vesely, F.

Djavanroodi, Investigating the Microstructure and Mechanical Properties of Aluminum-Matrix Reinforced-Graphene Nanosheet Composites Fabricated by Mechanical Milling and Equal-Channel Angular Pressing, Nanomaterials (Basel) 9(8) (2019) 1070-1087. https://doi.org/10.3390/nano9081070

[31] R. Shu, X. Jiang, J. Li, Z. Shao, D. Zhu, T. Song, Z. Luo, Microstructures and mechanical properties of Al-Si alloy nanocomposites hybrid reinforced with nano-carbon and in-situ Al_2O_3, Journal of Alloys and Compounds 800 (2019) 150-162. https://doi.org/10.1016/j.jallcom.2019.06.030

[32] C. Petit, J. Burress, T.J. Bandosz, The synthesis and characterization of copper-based metal–organic framework/graphite oxide composites, Carbon 49(2) (2011) 563-572. https://doi.org/10.1016/j.carbon.2010.09.059

[33] K.D. Woo, H.B. Lee, Fabrication of Al alloy matrix composite reinforced with subsive-sized Al_2O_3 particles by the in situ displacement reaction using high-energy ball-milled powder, Materials Science and Engineering: A 449-451 (2007) 829-832. https://doi.org/10.1016/j.msea.2006.02.402

[34] K.P. So, E.S. Kim, C. Biswas, H.Y. Jeong, D.H. Keum, K.H. An, Y.H. Lee, Low-temperature solid-state dissolution of carbon atoms into aluminum nanoparticles, Scripta Materialia 66(1) (2012) 21-24. https://doi.org/10.1016/j.scriptamat.2011.09.031

[35] M.S. Arab, N. El Mahallawy, F. Shehata, M.A. Agwa, Refining SiCp in reinforced Al–SiC composites using equal-channel angular pressing, Materials & Design 64 (2014) 280-286. https://doi.org/10.1016/j.matdes.2014.07.045

[36] J. Zhang, H. Yu, S.B. Kang, J.H. Cho, G. Min, V.Y. Stetsenko, Effect of fine-grained structural Al–12%Si materials on morphologies and crystal defects of eutectic Si in HCC Al–12%Si alloy billets, Journal of Alloys and Compounds 541 (2012) 157-162. https://doi.org/10.1016/j.jallcom.2012.05.030

[37] X. Qu, F. Wang, C. Shi, N. Zhao, E. Liu, C. He, F. He, In situ synthesis of a gamma-Al_2O_3 whisker reinforced aluminium matrix composite by cold pressing and sintering, Materials Science and Engineering: A 709 (2018) 223-231. https://doi.org/10.1016/j.msea.2017.10.063

[38] Y. Huang, P. Bazarnik, D. Wan, D. Luo, P.H.R. Pereira, M. Lewandowska, J. Yao, B.E. Hayden, T.G. Langdon, The fabrication of graphene-reinforced Al-based nanocomposites using high-pressure torsion, Acta Materialia 164 (2019) 499-511. https://doi.org/10.1016/j.actamat.2018.10.060

[39] J. Li, X. Zhang, L. Geng, Effect of heat treatment on interfacial bonding and strengthening efficiency of graphene in GNP/Al composites, Composites Part A: Applied Science and Manufacturing 121 (2019) 487-498. https://doi.org/10.1016/j.compositesa.2019.04.010

[40] X. Gao, H. Yue, E. Guo, H. Zhang, X. Lin, L. Yao, B. Wang, Preparation and tensile properties of homogeneously dispersed graphene reinforced aluminum matrix composites, Materials & Design 94 (2016) 54-60. https://doi.org/10.1016/j.matdes.2016.01.034

[41] M.D. Sangid, T. Ezaz, H. Sehitoglu, I.M. Robertson, Energy of slip transmission and nucleation at grain boundaries, Acta Materialia 59(1) (2011) 283-296. https://doi.org/10.1016/j.actamat.2010.09.032

[42] D. Scotto D'Antuono, J. Gaies, W. Golumbfskie, M.L. Taheri, Grain boundary misorientation dependence of β phase precipitation in an Al–Mg alloy, Scripta Materialia 76 (2014) 81-84. https://doi.org/10.1016/j.scriptamat.2014.01.003

[43] Y. Lang, Y. Cai, H. Cui, J. Zhang, Effect of strain-induced precipitation on the low angle grain boundary in AA7050 aluminum alloy, Materials & Design 32(8-9) (2011) 4241-4246. https://doi.org/10.1016/j.matdes.2011.04.025

[44] Q. Li, T. Xia, Y. Lan, W. Zhao, L. Fan, P. Li, Effect of in situ γ-Al2O3 particles on the microstructure of hypereutectic Al–20%Si alloy, Journal of Alloys and Compounds 577 (2013) 232-236. https://doi.org/10.1016/j.jallcom.2013.04.043

[45] M. Zuo, D. Zhao, X. Teng, H. Geng, Z. Zhang, Effect of P and Sr complex modification on Si phase in hypereutectic Al–30Si alloys, Materials Design 47 (2013) 857-864. https://doi.org/10.1016/j.matdes.2012.12.054

[46] Q. Liu, L. Ke, F. Liu, C. Huang, L. Xing, Microstructure and mechanical property of multi-walled carbon nanotubes reinforced aluminum matrix composites fabricated by friction stir processing, Materials & Design 45 (2013) 343-348.

https://doi.org/10.1016/j.matdes.2012.08.036

[47] S.R. Bakshi, D. Lahiri, A. Agarwal, Carbon nanotube reinforced metal matrix composites - a review, International Materials Reviews 55(1) (2010) 41-64. https://doi.org/10.1179/095066009x12572530170543

[48] R. Lapovok, D. Tomus, C. Bettles, Shear deformation with imposed hydrostatic pressure for enhanced compaction of powder, Scripta Materialia 58(10) (2008) 898-901. https://doi.org/10.1016/j.scriptamat.2008.01.010

[49] S. Zhao, Z. Zheng, Z. Huang, S. Dong, P. Luo, Z. Zhang, Y. Wang, Cu matrix composites reinforced with aligned carbon nanotubes: Mechanical, electrical and thermal properties, Materials Science and Engineering: A 675 (2016) 82-91. https://doi.org/10.1016/j.msea.2016.08.044

[50] P. Van Trinh, N. Van Luan, P.N. Minh, D.D. Phuong, Effect of Sintering Temperature on Properties of CNT/Al Composite Prepared by Capsule-Free Hot Isostatic Pressing Technique, Transactions of the Indian Institute of Metals 70(4) (2016) 947-955. https://doi.org/10.1007/s12666-016-0886-8

[51]B. Mani, M. Jahedi, M.H. Paydar, Consolidation of commercial pure aluminum powder by torsional-equal channel angular pressing (T-ECAP) at room temperature, Powder Technology 219 (2012) 1-8. https://doi.org/10.1016/j.powtec.2011.11.034

[52] M. Jahedi, M.H. Paydar, Three-dimensional finite element analysis of torsion extrusion (TE) as an SPD process, Materials Science and Engineering: A 528(29-30) (2011) 8742-8749. https://doi.org/10.1016/j.msea.2011.08.055

[53] R.E. Stoller, S.J. Zinkle, On the relationship between uniaxial yield strength and resolved shear stress in polycrystalline materials, Journal of Nuclear Materials 283 (2000) 349-352. https://doi.org/10.1016/S0022-3115(00)00378-0

[54] J.G. Park, D.H. Keum, Y.H. Lee, Strengthening mechanisms in carbon nanotube-reinforced aluminum composites, Carbon 95 (2015) 690-698. https://doi.org/10.1016/j.carbon.2015.08.112

[55] K. Nakashima, Z. Horita, M. Nemoto, T.G. Langdon, Development of a multi-pass facility for equal-channel angular pressing to high total strains, Materials Science and Engineering: A 281(1-2) (2000) 82-87. https://doi.org/10.1016/S0921-5093(99)00744-